Structure sensitivity of the oxidative activation of methane over MgO model catalysts: I. Kinetic study

Pierre Schwach, Wiebke Frandsen, Marc Willinger, Robert Schlögl, and Annette Trunschke*

Department of Inorganic Chemistry, Fritz-Haber-Institut der Max-Planck-Gesellschaft e.V., Faradayweg 4-6, 14195 Berlin, Germany.

schwachp@fhi-berlin.mpg.de
frandsen@fhi-berlin.mpg.de
willinger@fhi-berlin.mpg.de
acsek@fhi-berlin.mpg.de
trunschke@fhi-berlin.mpg.de

Abstract

The role of surface structure and defects in the oxidative coupling of methane (OCM) was studied over magnesium oxide as a model catalyst. Pure, nano-structured MgO catalysts with varying primary particle size, shape and specific surface area were prepared by sol-gel synthesis, oxidation of metallic magnesium, and hydrothermal post treatments. The initial activity of MgO in the OCM reaction is clearly structure-sensitive. Kinetic studies reveal the occurrence of two parallel reaction mechanisms and a change in the contribution of these pathways to the overall performance of the catalysts with time on stream. The initial performance of freshly calcined MgO is governed by a surface-mediated coupling mechanism involving direct electron transfer between methane and oxygen. The two molecules are weakly adsorbed at structural defects (steps) on the surface of MgO. The proposed mechanism is consistent with high methane conversion, a correlation between methane and oxygen consumption rates, and high C_2H_4 selectivity after short times on stream. The water formed in the OCM reaction causes sintering of the MgO particles and loss of active sites by degradation of structural defects, which is reflected in decreasing activity of MgO with time on stream. At the same time, gas-phase chemistry becomes more important, which includes formation of ethane by coupling of methyl radicals formed at the surface and the partial oxidation of C_2H_6. The mechanistic concepts proposed in this work (Part I) will be substantiated in Part II by spectroscopic characterization of the catalysts.[1]

Keywords

MgO; oxidative coupling; methane; ethane; ethylene; defects; reaction mechanism

1. Introduction

Activation of methane over heterogeneous catalysts remains an attractive subject in view of the abundance of natural gas and renewable methane resources. The scientific interest in oxidative coupling of methane (OCM) to ethane, ethylene, and higher hydrocarbons (C_{2+} products), however, went down noticeably during the past years. One reason might be that in spite of numerous attempts using chemically quite different catalysts, C_{2+} yields of about 30 % have not been significantly surpassed so far. In addition, the diversity of known active catalyst masses complicates the identification of a general functional model.[2] The not yet fully resolved relationship between surface and gas phase chemistry of CH_4 at the high reaction temperatures inspired us to deal with fundamental questions of methane activation on the surface of heterogeneous catalysts in a systematic approach addressing in particular the function of surface defects using magnesium oxide as a model.

Li-doped MgO was discovered by Lunsford *et al.* as an active catalyst in the oxidative coupling of methane using molecular oxygen 28 years ago.[3] The originally proposed reaction mechanism involves the activation of gas-phase O_2 on either intrinsic cationic vacancies on the surface of Li-free MgO or on substitutional Li^+ ions under formation of O^- or $[Li^+O^-]$ centers, respectively,[3, 4] which can abstract a hydrogen atom from methane. The resulting methyl radical is released to the gas phase to undergo selective coupling to ethane. The selectivity could be to a large extent governed by consecutive reactions, since methyl radicals may not exclusively collide with themselves. By reaction with gas phase oxygen or with O^{2-} ions on the catalyst surface, $CH_3O_2^{\cdot}$ radicals or surface methoxy species CH_3O^- can be formed, respectively, which are considered as intermediates in the undesired formation of CO_2 that limits the C_{2+} yield. The mechanism, which has been proposed by Lunsford *et al.* for MgO and Li-MgO, has been, meanwhile, applied to chemically very different catalysts.[5]

The outstanding activity of Li-MgO catalysts compared to pure MgO in methane activation has been explicitly attributed to the presence of the specific $[Li\text{-}O]^-$ centers.[6] However, lithium as a fluxing agent causes sintering of magnesium oxide at the high reaction temperatures.[6] A clear impact of the varying morphology of MgO, which changes in the course of the sintering process, on undesired secondary surface reactions of re-adsorbed methyl radicals was not observed.[6] In return it was shown that lithium, which completely desorbs by formation of volatile compounds during the oxidative pretreatment of the catalyst (which involves the loss of all $[Li\text{-}O]^-$ centers), acts as a structural promoter that favors the formation of terminating higher index planes like {111} or {110}.[2, 7] The highest selectivity to C_{2+} products was found for pure MgO catalysts, which expose a greater fraction of {111} planes.[8]

Inconsistent findings have also been reported with respect to activity. From studies of magnesium oxide catalysts, which show similar morphology, but different cube size, it was concluded that edge and corner sites are not catalytically significant under steady state conditions.[8] However, Ito *et al.* reported that low coordination ions on the surface of MgO play an important role in the dissociation of adsorbed methane.[9]

Defects will definitely fulfill a key function with respect to the activation of either methane or oxygen by changing the electronic structure of the wide band gap magnesium oxide particularly with regard to facilitate the transfer of electrons between the solid surface and the adsorbed molecules, which undergo a redox reaction.[10-15] The present work addresses relations between the nature and abundance of morphological surface defects such as steps and corners on pure magnesium oxide and its reactivity in the oxidative coupling of methane. Various synthetic techniques have been applied to prepare nano-structured MgO catalysts with different morphology. In part I of this work, we will report about synthesis, microstructural, and kinetic analysis of the morphologically different MgO catalysts. Part II

deals with the spectroscopic investigation of coordinatively unsaturated surface sites and the electronic structure. We propose a reaction path for the activation of methane on freshly activated MgO that is confirmed by the detection of reaction intermediates using EPR spectroscopy. The observed fast deactivation of magnesium oxide is interpreted in terms of a change from a concerted reaction that involves co-adsorption of methane and oxygen on mono-atomic step sites to a sequential reaction in which methane and oxygen are activated independently. The latter scenario dominates under steady-state conditions.

2. Experimental

2.1. Starting materials

Magnesium chips (99.98 %, Sigma Aldrich), magnesium oxide (Puratronic®, 99.99 %, Alfa Aesar), methanol (ROTIPURAN®, ≥99.9%, p.a., ROTH), and toluene (ROTIPURAN®, ≥99.9%, p.a., ROTH) were used as received. Ultrapure water was obtained by using the Milli-Q Synthesis System (MQ). All gases for the catalytic reaction were purchased at Westfalen AG. The purity of nitrogen, argon, and oxygen was 99.999 %, the purity of hydrocarbons was 99.95 %.

2.2. Catalyst synthesis

Magnesium oxide was prepared applying various dry and wet methods starting with metallic Mg or MgO. Purchased MgO (C-MgO) is used as reference and raw material for surface modification.

By oxidation of Mg in air, the so-called “smoke” (S) magnesium oxide (S-MgO) was obtained. The generated oxide particles were collected using a glass funnel.

Starting from metallic Mg, but following a sol-gel (SG) procedure,[16] SG-MgO was prepared by dissolving 7 g Mg in 300 mL methanol under argon and stirring at T=273 K. The

resulting solution of $Mg(OCH_3)_2$ was diluted with 1 liter toluene and hydrolysis was initiated by adding 11 g water (0.61 mol, 2 eq) drop-wise under stirring at the same temperature. The solution was aged for 12 h at T=295 K until a gel was formed. A fraction of 180 mL of the gel was then placed in a Teflon-lined 300 mL autoclave (Parr GmbH). The autoclave was first purged and then pressurized to 7 bar with N_2. Subsequently, the gel was heated in the closed autoclave to 538 K applying a heating rate of 1 K/min. After 3 hours the pressure achieved 70 bar. The system was allowed to equilibrate at 538 K for 10 min. Then, the heater was switched off and the pressure was released within 1 min. The obtained $Mg(OH)_2$ aerogel was further dried in air at 393 K for 12 h.

Purchased magnesium oxide (C-MgO) was modified by hydrothermal treatment (HT) in water at normal pressure. For this purpose, 5 grams of C-MgO were treated in 500 mL of distilled water at T=373 K under reflux for 16 h. After cooling to room temperature, the suspension was filtered and washed with distilled water. The powder was dried at 393 K for 12 h giving the precursor of HT-MgO.

Hydrothermal treatment of C-MgO was also performed under pressure using microwave (MW) heating. Two Teflon autoclaves with a volume of 80 mL were filled each with 5 grams of C-MgO suspended in 60 mL of distilled water and heated to 483 K for 3 hours in a microwave (Speedwave MWS-3+, Berghof Products + Instruments GmbH). The resulting suspension was filtered and washed with distilled water. The obtained material was dried at 393 K in air for 12 h yielding the precursor of MW-MgO.

All synthesis techniques result in $Mg(OH)_2$ or MgO-$Mg(OH)_2$ phase mixtures which were transformed into the oxide by calcination in a O_2/Ar (20/80) atmosphere applying a flow of 150 mL/min. The precursor (3 g) was placed into a ceramic crucible, which was positioned into a quartz tube. The calcination was performed at 1123 K (3 $K \cdot min^{-1}$) for 6 hours. The

resulting catalysts were stored under argon and freshly pre-treated before analysis or catalysis as described in the following sections.

2.3. Nitrogen adsorption

The surface area determination was carried out in a volumetric N_2 physisorption set-up (Autosorb-6-B, Quantachrome) at the temperature of liquid nitrogen. The sample was degassed in dynamic vacuum at a temperature of 473 K for 2 h prior to adsorption. Full adsorption and desorption isotherms were measured. The linear range of the adsorption isotherm (p/p_0=0.05–0.3) was considered to calculate the specific surface area according to the BET method.

2.4. X-ray diffraction

The X-ray diffraction (XRD) measurements were performed in Bragg-Brentano reflection geometry on a Bruker AXS D8 Advance theta/theta diffractometer equipped with a secondary graphite monochromator (Cu $K\alpha_1$ radiation, λ=1.5406 Å) and scintillation detector. The sample powder was filled into the recess of a cup-shaped sample holder, the surface of the powder bed being flushed with the sample holder edge. Diffraction patterns were recorded in the range 20–90° 2θ with a step size of 0.02° and an accumulation time of 15 s/step. The XRD data were analyzed by full pattern fitting using the TOPAS software (version 3, copyright 1999, 200 Bruker AXS).

2.5. Elemental analysis

Metal impurities were analyzed by inductively coupled plasma–optical emission spectrometry (ICP-OES) using an ICP-OES 6000 Series spectrometer (Thermo). The samples were dissolved in 10 mL of 66 % HNO_3 for 6 hours at 458 K.

2.6. Electron microscopy

Transmission electron microscopy (TEM) was performed using a Philips CM 200 instrument. The microscope is equipped with a field emission gun and was operated at 200kV. Samples for TEM were prepared in a dry way, *i.e.* without dispersing the particles in a solvent. Instead, the copper TEM grids were dipped into the MgO powder. This method prevents alteration or contamination of the sample. After tapping off excessive material, enough particles generally remained attached to the holy carbon support film of the grid for TEM investigation. SEM was performed using a Hitachi S4500 field emission scanning electron microscope.

2.7. Oxidative coupling of methane

The catalytic measurements were carried out in a laboratory fixed bed reaction system designed to investigate partial oxidation of hydrocarbons. The reactor consists of a quartz U-tube (4 mm inner diameter, 6 mm outer diameter, 26 cm length). The inner diameter of the tube downstream the catalyst bed is reduced to 1 mm in order to minimize the influence of gas phase reactions. The reactor is heated using a tube furnace (Carbolite®). An axial K-Type thermocouple inserted in a ceramic jacket was placed just above the catalyst bed for measurement of input gas temperature. To avoid condensation of products (*e.g.* water) the reactors, part of the gas delivery system and the gas sampling system are placed in a heating cabinet that is usually kept at 353 K. N_2, O_2, hydrocarbons, and any other gases of interest are mixed outside of the heating cabinet via mass flow controllers (EL-FLOW, Bronkhorst).

The catalysts were pressed and sieved resulting in a sieve fraction of 200-300 µm, and used undiluted when studied at a contact time of 0.033 $g \cdot s \cdot ml^{-1}$ (results shown in Table 3). In all other measurements the catalysts were diluted with 150 mg SiC composed of

the same sieve fraction as the catalysts. The reaction conditions are indicated in the legends of the figures. The catalytic bed height varied between 1.3 and 1.1 cm depending on the amount of catalyst and SiC used. The catalysts were heated to reaction temperature in N_2 and kept at this temperature for one hour prior switching to the feed.

Gas analysis was performed online by gas chromatography (gas chromatograph 6890A, Agilent) equipped with two channels. A combination of two capillary columns (GS-CarbonPLOT (length 30 m, 0.53 mm inner diameter, 40 µm film thickness), and HP-PLOT Molesieve/5A (length 30 m, 0.53 mm inner diameter, 25 µm film thickness)) in connection with a thermal conductivity detector (TCD) was used to analyse the permanent gases CO_2, O_2, N_2, and CO. A combination of two capillary columns (HP-FFAP (length 30 m, 0.53 mm inner diameter, 1 µm film thickness), and HP-PLOT Q (length 30 m, 0.53 mm inner diameter, 40 µm film thickness)) connected to a flame ionization detector (FID) is used to analyse alkanes, olefins, and oxygenates (*e.g.*, CH_4, C_2H_6, C_2H_4, C_3H_8, and C_3H_6).

The catalytic experiments were carried out in such a way that the common criteria for a plug flow model were fulfilled, *i.e.*:

$$\frac{L}{d_p} > 50\,,\ \frac{d_r}{d_p} > 10\,,\ \frac{L}{d_r} > 5 \qquad \text{equation (1)}$$

with L being the length of the catalytic bed, d_r the diameter of the reactor (4 mm) and d_p the diameter of the catalyst particles (0.3-0.2 mm).

Considering the mass balance, the following expression was used to determine the rate of the reaction with respect to the substrate or product *i* at steady-state*:*

$$\frac{dc_i}{d\left(\frac{W}{F^o}\right)} = -\nu_i r_i \qquad \text{equation (2)}$$

with W the weight of the catalyst (in g), $F°$ the flow of the reactants (in ml/s), r_i the reaction rate of consumption or formation, ν_i the stoichiometric coefficient, and c_i the concentration of the reactants or products.

Nitrogen was used as internal standard to account for volume effects due to the high temperature, at which the reaction is performed, on the gas phase analysis.

The conversion of oxygen was calculated as follows:

$$X_{O_2} = \frac{\frac{c_{O_2,in}}{c_{N_2,in}} - \frac{c_{O_2,out}}{c_{N_2,out}}}{\frac{c_{O_2,in}}{c_{N_2,in}}} \qquad \text{equation (3)}$$

with $c_{02,in}$ the concentration of oxygen at the inlet of the reactor and $c_{02,out}$ the concentration of oxygen at the outlet of the reactor.

The conversion of methane was calculated based on the sum of products:

$$X_{CH_4} = \frac{\sum\left(\frac{n_{carbon-atoms,i}}{n_{carbon-atoms,CH_4}} c_{i,out}\right) - c_{CH_4,out}}{\sum\left(\frac{n_{carbon-atoms,i}}{n_{carbon-atoms,CH_4}} c_{i,out}\right)} \qquad \text{equation (4)}$$

with $n_{cabon\text{-}atoms,i}$ the number of carbon atoms in the hydrocarbon product *i*.

Selectivity was calculated including the number of carbon atoms, rather than stoichiometric coefficients, and the sum of products found:

$$S_i = \frac{\frac{n_{carbon-atoms,i}}{n_{carbon-atoms,CH_4}} c_{i,out}}{\sum\left(\frac{n_{carbon-atoms,i}}{n_{carbon-atoms,CH_4}} c_{i,out}\right)} \qquad \text{equation (5)}$$

The mass balance of carbon was 100±1.5% indicating that species containing more than 4 carbon atoms or oxygenated species were formed only in negligible quantities.

The absence of transport limitations was verified by dimensionless criteria based on the film diffusion model,[17] using the approximations that (i) the pellets are ideal spheres and (ii) the particle tortuosity factor is determined by the particle porosity $\tau_p=\varepsilon_p^{-0.5}$. The dimensionless parameters where calculated for methane and oxygen in the feed mixture revealing no mass or heat transport limitations at any of the applied experimental conditions under steady-state conditions. In the absence of mass transport limitations the Carberry number and the Wheeler-Weisz criterion have to be lower than 0.05 and 0.1, respectively. In the current experiments the highest calculated Carberry number was 0.0014, and the highest Wheeler-Weisz criterion was 0.05. For extra- and intra-particle heat transport the maximum calculated values were 0.0028 and $2.45\cdot10^{-4}$, respectively, and both criteria were lower than 0.05. The maximum calculated temperature difference between the bed near the wall of the reactor and the average temperature in the bed is 2.4 K, which is lower than the maximum allowed temperature difference of 4.8 K.

In summary, the kinetic data obtained in this paper are free of mass and heat transport limitation effects and represent the intrinsic kinetics of the catalysts tested.

3. Results

3.1. Synthesis of nano-structured MgO catalysts

Different preparation methods and post-synthetic treatments have been applied with the objective to obtain magnesium oxide nano-particles with varying primary particle size, shape, and surface area. Sol-gel synthesis (SG-MgO), and oxidation of metallic magnesium (S-MgO) were used starting from metallic magnesium. Furthermore, commercially available

magnesium oxide (C-MgO) was modified by hydrothermal treatment at normal pressure (HT-MgO), and at elevated pressure in a microwave autoclave (MW-MgO).

The surface area of the freshly calcined catalysts, which have been pressed and sieved prior to the catalytic reaction into split of a sieve fraction of 0.2-0.3 mm, varies by an order of magnitude between 12 $m^2 \cdot g^{-1}$ for S-MgO and 111 $m^2 \cdot g^{-1}$ for MW-MgO (Table 1). The increase in specific surface area is not directly reflected in a decrease of the mean crystallite size determined by XRD indicating that surface texturing contributes substantially to the surface area measured by nitrogen adsorption, in particular for the catalysts prepared by hydrothermal post treatment and sol-gel synthesis.

Table 1
Specific surface area and domain size determined by XRD of MgO catalysts before and after use in oxidative coupling of methane.

Catalyst name	Preparation method	Calcined catalysts[a]				Catalysts after use in OCM[b]			
		Catalyst ID[c]	S_{BET} [m^2g^{-1}]	D_{XRD} [nm]	a [Å]	Catalyst ID[c]	S_{BET} [m^2g^{-1}]	D_{XRD} [nm]	a [Å]
S-MgO	Combustion	12817	11.6	85.0	4.2144	12992	7.6	67.3	4.2135
C-MgO	Reference	12288	19.1	23.1	4.2145	12798	7.9	77.3	4.2145
SG-MgO	Sol-gel	12342	38.6	11.4	4.2175	12500	6.8	84.9	4.2155
HT-MgO	Hydrothermal	12498	71.6	14.4	4.2177	12628	n.a.	n.a.	n.a.
MW-MgO	Microwave	12994	111.0	13.3	4.2176	13036	12.2	70.5	4.2138

[a] O_2/Ar = 20/80, 150 mL/min^{-1}, heating rate 3 K/min^{-1}, T=1123 K, t=6 h.
[b] $CH_4/O_2/N_2$=3/1/1, W/F=0.15 g·s·ml^{-1}, T= 1073 K, after approximately 300 h TOS.
[c] The catalyst ID is required to clearly identify the batch number of various reproductions of catalyst synthesis

The purity of the catalysts was controlled by chemical analysis (Table 2). The total concentration of transition metal ions, especially iron, chromium, and manganese, does not exceed 10 ppm for the materials that are derived from ultra-pure C-MgO. The content of calcium and sodium is slightly higher. Practically no additional metals are introduced by subsequent hydrothermal treatments that lead to the catalysts HT-MgO and MW-MgO. The

comparatively high Ca, Na, and Fe contents of S-MgO and SG-MgO (46 ppm) results from the use of commercial magnesium that was not purified by distillation

Table 2
Content of traces of metal impurities as determined by using inductively coupled plasma–optical emission spectrometry (ICP–OES).

Catalyst	Metal impurities [ppm]								
	Ca	Na	Cr	Mn	Fe	Co	Ni	Cu	Zn
S-MgO	212.3	201.20	3.79	6.53	30.26	0.18	1.89	7.22	4.80
C-MgO	9.70	20.70	0.17	2.96	3.80	0.06	0.14	0.50	1.44
SG-MgO	10.10	36.40	8.35	10.35	46.27	0.05	6.82	4.04	1.60
HT-MgO	8.90	26.30	0.12	2.90	3.21	0.06	0.13	0.91	1.60
MW-MgO	6.20	25.40	0.23	3.09	2.64	0.17	0.22	0.60	1.54

The morphology and microstructure of the calcined catalysts was analyzed by electron microscopy (Fig. 1, left column). All catalysts expose mainly {100} faces,[18] but clearly differ with respect to size, shape and the abundance of steps and corners.

The oxidation of metallic magnesium in air produces large, almost ideal cubic particles, exhibiting mainly {100} faces (S-MgO, Fig. 1A). The particles are partially aggregated via shared faces. Due to large size and flat surfaces, S-MgO exhibits a low specific surface area of 12 $m^2 \cdot g^{-1}$. The average crystallite size determined by XRD is around 85 nm, however, scanning electron microscopy indicates a rather broad size distribution with particles in the range between 50 and 200 nm (Fig. S1A). Such poly-disperse powders are often obtained by combustion of metallic magnesium in air.[19]

The specific surface area of C-MgO after calcination at 1123 K is also relatively small (Table 1). The side length of the crystallites observed by TEM (Fig. 1C) is approximately 20-30 nm, which is in agreement with the mean crystallite size of 23 nm measured by XRD. The primary particles are of regular cubic morphology exposing {100} faces with sharp edges and corners.

The height of the steps that often appear close to the edges of the cubes is in the nanometer range. Smaller steps, in the range of just few Ångströms and eventually even in the dimension of one Mg-O distance (mono-atomic steps) can regularly be observed within the {100} faces. The primary particles are agglomerated or aggregated to form clusters up to 5 μm in size (Fig. S1C).

Magnesium oxide obtained by sol-gel synthesis (SG-MgO) has a larger surface area of 39 $m^2 \cdot g^{-1}$ and a smaller mean crystallite size of ca. 11 nm. TEM (Fig. 1E) and SEM (Fig. S1E) images reveal rectangular primary particles with a side length of approximately 20 nm and a narrow size distribution. The microstructure of SG-MgO is quite similar to C-MgO. Agglomerates or aggregates of primary particles comprise a cluster size of approximately 5 μm.

MgO catalysts obtained by hydrothermal treatment of C-MgO either at normal pressure (HT-MgO) or in a microwave-heated autoclave (MW-MgO) are characterized by substantial nano-structuring of the surface. Whereas the mean crystallite size of the two catalysts is comparable to C-MgO or SG-MgO (Table 1), surface roughness is reflected in high surface areas. The regular cubic structure of the starting material C-MgO is no longer visible by TEM (Figs. 1G and 1I). Conglomerates without distinguishable primary particles are embedded in clusters of a size of ca. 1 μm (Figs. S1G, and S1H).

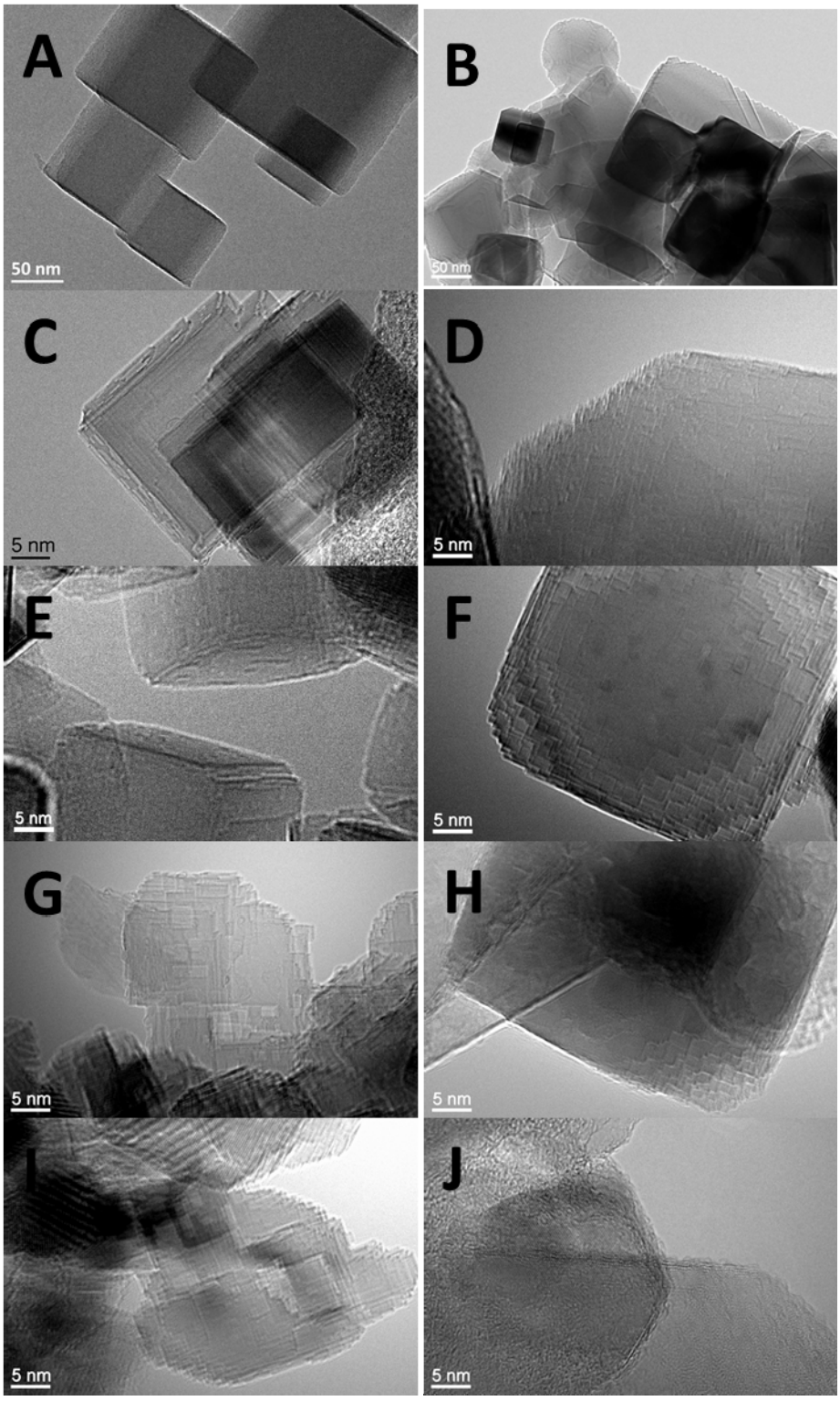

Fig. 1. TEM images of calcined MgO (on the left-hand side) and MgO after oxidative coupling of methane for 300 hours time on stream ($CH_4/O_2/N_2$=3/1/1, W/F=0.15 g·s·ml^{-1}, T= 1073 K) (on the right-hand side). From top to bottom: S-MgO (A,B), C-MgO (C,D), SG-MgO (E,F), HT-MgO (G,H), and MW-MgO (I,J).

Sintering phenomena are observed for all catalysts after use in the oxidative coupling of methane at 1073 K for approximately 300 hours time on stream. The domain size determined by XRD increases substantially except in the case of S-MgO, that shows a slight size reduction of the initially very large particles (Table 1). In agreement with a similar size of the coherently scattering domains in the used catalysts, the specific surface area of all used catalysts is similar and varies between 7 and 12 $m^2 \cdot g^{-1}$. Sintering is also visible by TEM (Fig. 1, right column) and SEM (Fig. S1, right column). After catalysis, the morphology of the primary particles is much more rounded. The characteristic sharp edges and corners of the cubic structure have disappeared and pseudo {110} as well as {111} faces consisting of stepped edges between {100} planes and numerous corners have been formed.

3.2. Oxidative coupling of methane

3.2.1. Catalyst deactivation

The five MgO materials were investigated in the oxidative coupling of methane (OCM). For a better comparison with the kinetic data in the literature, the experimental condition for the OCM reaction were chosen similar to the reference work of Schweer *et al.*.[20] The catalysts experience a strong deactivation with time on stream (TOS) until steady-state activity is reached (Fig. 2). The time that is required to attain the steady-state varies between 1 hour and 230 hours depending on the method that has been applied to synthesize the MgO catalysts. Consequently, the deactivation rate seems to depend strongly on the initial structure of the magnesium oxide. The stability of the catalysts in the OCM reaction decreases in the following order: C-MgO>SG-MgO>MW-MgO>HT-MgO>S-MgO (Fig. 2). At 1073 K in a feed of $CH_4/O_2/N_2$=3/1/1 and applying a contact time of W/F= 0.150 $g \cdot s \cdot ml^{-1}$, full conversion of oxygen is achieved for all MgO catalysts (except for S-MgO) in the initial state of the reaction after a few minutes time on stream. Under conditions of total oxygen consumption,

the methane conversion results in a maximum of 30 % for all affected catalysts (Fig. 2A). The selectivity to C_{2+} products decreases with time on stream, but in most of the cases only slightly (Fig. 2B).

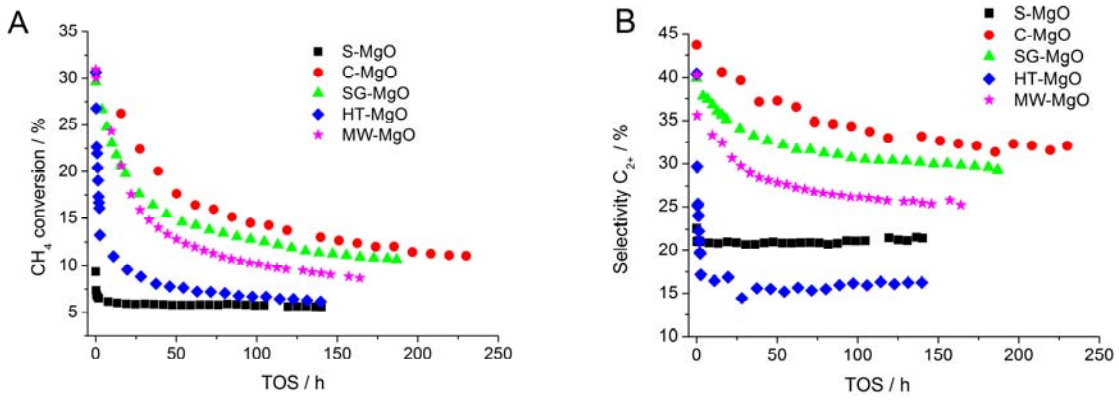

Fig. 2. Changes in the conversion of methane (A) and in the selectivity to C_{2+} products (B) with time on stream in the oxidative coupling of methane at T=1073 K in a feed of $CH_4/O_2/N_2$=3/1/1 using a catalyst mass of m_{cat}=150 mg, and applying a contact time of W/F= 0.150 $g \cdot s \cdot ml^{-1}$ over the differently prepared MgO catalysts.

With time on stream, the ratio of ethylene to ethane decreases at the similar rate as the methane conversion decreases (Fig. 3A). The carbon dioxide to carbon monoxide ratio declines at a much faster rate (Fig. 3B). Fig. 4 emphasizes in another way the change of selectivity with time of stream for the C-MgO catalyst. The decrease in selectivity to C_2H_4 is accompanied by a decrease in CO_2 selectivity, while C_2H_6 and CO follow the opposite trend. This indicates changes in the reaction pathway with time on stream, but it has to be considered that the formation of the products and the consumption of intermediates are interrelated within a complex reaction network.

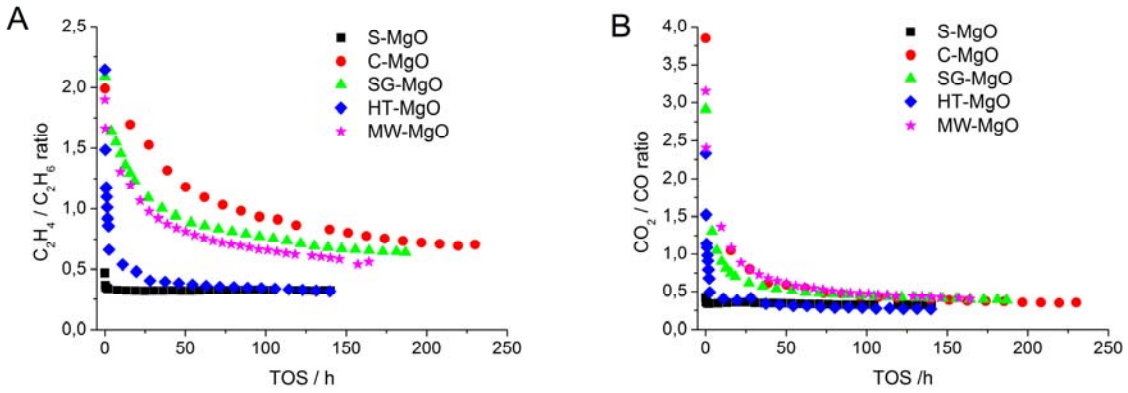

Fig. 3. Changes in the selectivity ratio ethylene/ethane (A), and CO_2/CO (B) with time on stream in the same experiments as presented in Fig. 2.

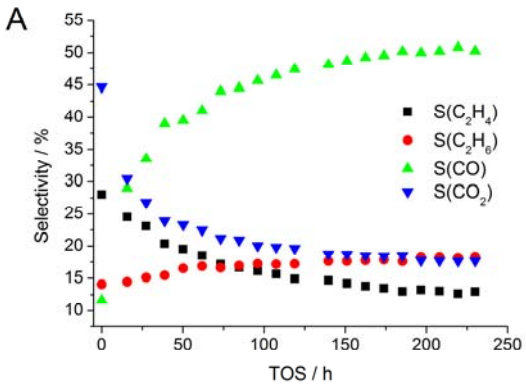

Fig. 4. Changes in the selectivity to the products ethylene, ethane, CO, and CO_2 with time on stream exemplarily shown for catalyst C-MgO in the same experiments as presented in Fig. 2.

In order to investigate relations between particle morphology, specific surface area, and reactivity, the C-MgO catalyst was analyzed after 6, 20 and 66 hours time on stream by TEM and nitrogen adsorption (Fig. 5). The MgO particles are attacked at first at the outer surface of the primary cubic particles exposing {100} planes and many steps. With time on stream the cubic particles are transformed into particles exhibiting an octahedral shape (Fig. 5B). After 20 hours time on stream, the size of the particles becomes larger but steps and corners can still be recognized (Fig. 5C). After 66 hours time on stream the particles are completely rounded and no {100} structure can be observed (Fig. 5D). With increasing particle size, the surface area decreases as indicated in the caption of Fig. 5.

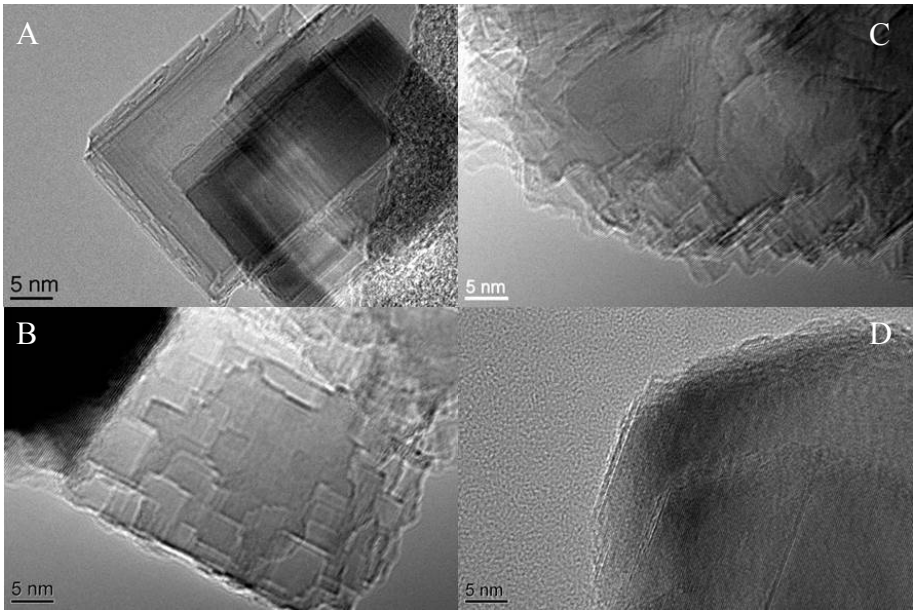

Fig. 5. TEM images of C-MgO at different time on stream in the OCM reaction, same experimental condition as in Fig. 2. A) Before reaction, B) after 6 h TOS (S_{BET}=22.3 $m^2 \cdot g^{-1}$), C) after 20 h TOS (S_{BET}=16.4 $m^2 \cdot g^{-1}$), D) after 66 h TOS (S_{BET}=15.0 $m^2 \cdot g^{-1}$).

3.2.2. Initial performance at incomplete oxygen conversion

Under the reaction conditions applied in the previous section, total oxygen consumption was observed at time *t=0* in the case of HT-, MW-, C-, and SG-MgO. As a consequence, the methane conversion results in a maximum conversion of ca. 30 % for all catalysts except S-MgO that shows lower methane conversion. Similar selectivity towards C_{2+} hydrocarbons of ca. 40 % is observed for all catalysts, which renders a comparison of the catalysts at *t=0* impossible. To overcome this limitation, the catalysts were tested at lower contact time (W/F = 0.033 $g \cdot s \cdot ml^{-1}$) and temperature (1023 K). The reactivity of all catalysts under these conditions is compared in Table 3 at *t=0*. The ***initial*** rates measured over the differently prepared MgO catalysts differ by an order of magnitude. MW-MgO exposes the highest consumption rate of methane, combined with the highest yield of C_{2+} hydrocarbons, and the highest ratios of CO_2/CO and C_2H_4/C_2H_6 selectivity, respectively. The selectivity ratios increase with increasing methane and oxygen conversion. The

methane consumption rate decreases in the order MW-MgO>SG-MgO>C-MgO>HT-MgO>S-MgO. The rates do not directly correlate with the specific surface areas of the catalysts. Therefore, normalization of the rates to the specific surface area changes the ranking with respect to activity. The specific rate decreases in the order C-MgO>SG-MgO>MW-MgO>S-MgO>HT-MgO.

Table 3
Consumption rate of methane, conversion, and selectivity measured over MgO catalysts in the oxidative coupling of methane in the ***initial*** state (*t=0*) at T=1023 K, applying a feed composition of $CH_4/O_2/N_2$=3/1/1, and a contact time of 0.033 g·s·ml^{-1}.

	$r(CH_4)$ [mol·s^{-1}·g$^{-1}_{cat}$]	$r(CH_4)$ [mol·s^{-1}·m$^{-2}_{cat}$]	$X(CH_4)$ [%]	$X(O_2)$ [%]	$S(C_{2+})$ [%]	CO_2/CO[a]	C_2H_4/C_2H_6[a]
S-MgO	16.3	1.41	2	5	5	0.25	0
C-MgO	185.2	9.70	23	75	28	1.10	0.72
SG-MgO	214.4	5.56	26	87	30	1.51	1.01
HT-MgO	65.0	0.91	8	27	5	0.40	0.19
MW-MgO	249.0	2.24	30	98	41	2.28	1.42

[a] ratio of selectivity

3.2.3. Steady-state performance

In the following, kinetic investigations in the ***steady-state*** are presented, which have been performed after reaching constant oxygen and methane conversion and selectivity at 1073 K in a feed of $CH_4/O_2/N_2$=3/1/1 using a catalyst mass of m_{cat}=150 mg and applying a contact time of W/F= 0.150 g·s·ml^{-1} (*i.e.*, after the experiment shown in Fig. 2). This takes 150-250 hours, depending on the catalyst preparation. The performance of the catalysts at steady state is summarized in Table 4.

Table 4
Consumption rate of methane, conversion, and selectivity measured over MgO catalysts in the oxidative coupling of methane in the ***steady-state*** at T=1023 K, applying a feed composition of $CH_4/O_2/N_2=3/1/1$, and a contact time of 0.15 g·s·ml^{-1}.

	$r(CH_4)$ [µmol·s^{-1}· g$^{-1}_{cat}$]	$r(CH_4)$ [µmol·s^{-1}· m$^{-2}_{cat}$]	$X(CH_4)$ [%]	$X(O_2)$ [%]	$S(C_{2+})$ [%]	CO_2/CO[a]	C_2H_4/C_2H_6[a]
S-MgO	4.17	0.55	2	11	9	0.39	0.07
C-MgO	10.43	1.32	6	15	17	0.25	0.24
SG-MgO	8.57	1.26	5	13	14	0.24	0.18
HT-MgO	4.72	n.a.	3	8	6	0.18	0.09
MW-MgO	7.38	0.60	4	13	11	0.26	0.19
SiC	0.25	n.d.	0.1	1.2	65	0.0	0.0

[a] ratio of selectivity

The comparison reveals that the differences between the catalysts in the steady state are much smaller compared to the differences in the initial performance. Still, C-MgO shows the highest specific activity and the ranking of the specific activity remains the same as the ranking of specific rates measured at *t=0*.

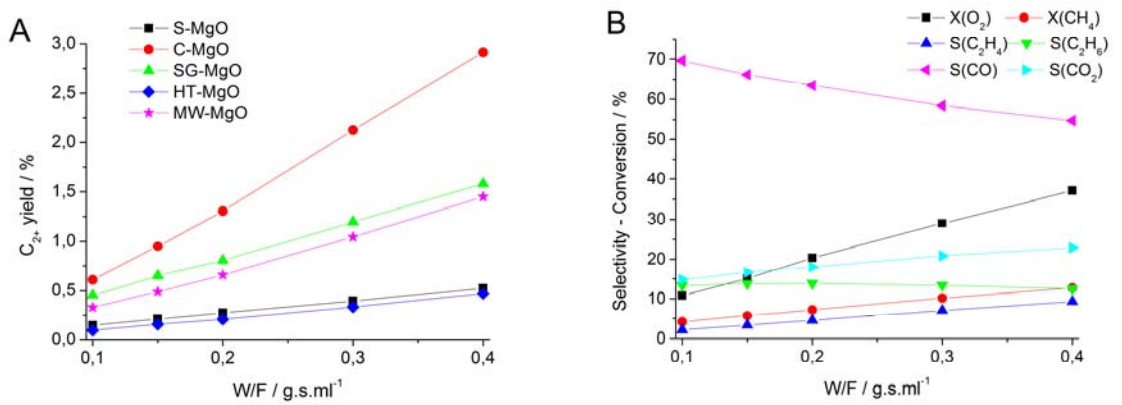

Fig. 6. Total yield of the coupling products ethane and ethylene for all catalysts (A), and conversion and selectivity exemplarily shown for C-MgO (B) as a function of the contact time at T=1023 K using a catalyst mass of m_{cat}=150 mg, and a feed composition of $CH_4/O_2/N_2=3/1/1$.

The detailed kinetic study under steady-state conditions comprising all five MgO catalysts reveals an interesting correlation between temperature, contact time, methane to oxygen ratio, and reactivity in the OCM reaction. First, in contrast to the work of Hargreaves *et al.*,[8] in which OCM over MgO was studied at the same reaction temperature, but at higher contact times and in slightly different feed, the contact time has a significant effect on methane conversion and selectivity to C_{2+} hydrocarbons, respectively (Figs. 6, S2-S5). The C_{2+} yield increases for all catalysts with increasing contact times (Fig. 6A), which is due to an increase in methane conversion and ethylene selectivity, while the CO selectivity decreases (Figs. 6B, S2-S5). In parallel, the oxygen conversion increases as well. The C_2H_6 selectivity is not affected. However, the increase in the C_{2+} yield is different for the various catalysts, which may also explain the discrepancy to the studies reported previously.[8] Whereas C-MgO shows a 6 times higher yield at W/F = 0.4 $mg \cdot s \cdot ml^{-1}$ than at W/F = 0.1 $mg \cdot s \cdot ml^{-1}$, the influence of the contact time on the yield is less pronounced for S-MgO and HT-MgO (Fig. 6A). The same trend becomes also evident from Fig. 7A, where the C_{2+} selectivity is plotted as a function of methane conversion that was changed by varying the contact time at a reaction temperature of T=1023 K in the same range and in the same steps in all experiments. The selectivity increases with increasing methane conversion for all catalysts. Fig. 7A illustrates also that at the same methane conversion, C-MgO shows the highest selectivity to coupling products followed by SG-MgO > MW-MgO = S-MgO > HT-MgO. The representation of the selectivity towards ethylene and ethane as a function of methane conversion for the C-MgO catalyst shows that when methane conversion increases (*i. e.* by increasing the contact time), the C_2H_4 selectivity increases linearly, while the C_2H_6 selectivity stays constant (Fig. 7B). This behavior is not in agreement with a reaction pathway, in which ethylene is formed from ethane through oxidative dehydrogenation. With increasing methane conversion, *i.e.* increasing W/F, the formation of C_3 hydrocarbons sets in, starting with

propylene followed by propane. For evaluation of the gas phase contributions under the same reaction conditions, silicon carbide was studied, that shows methane conversion below 1% (Fig. 8). The trends in ethylene and ethane selectivity over SiC clearly differ from the MgO catalysts. At low methane conversion only C_2H_6 is formed. At higher CH_4 conversion, ethane seems to be decomposed to CO and the formation of C_2H_4 occurs at even higher methane conversion accompanied by the formation of CO_2.

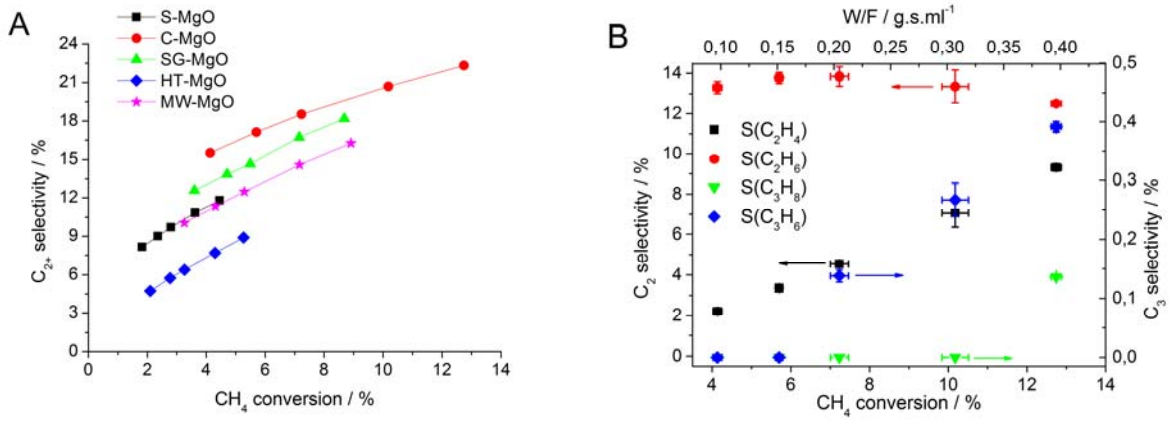

Fig. 7. Total selectivity to the coupling products ethane and ethylene as a function of methane conversion (A), and selectivity to C_2, and C_3 hydrocarbons exemplarily shown for catalyst C-MgO as a function of methane conversion (the error bars indicate an confidence interval of 99.73 % (3σ)) (B) measured at T=1023 K using a catalyst mass of m_{cat}=150 mg, and a feed composition of $CH_4/O_2/N_2$=3/1/1. The conversion was changed by variation of the contact time in the range between 0.1 and 0.4 g·s·ml^{-1}.

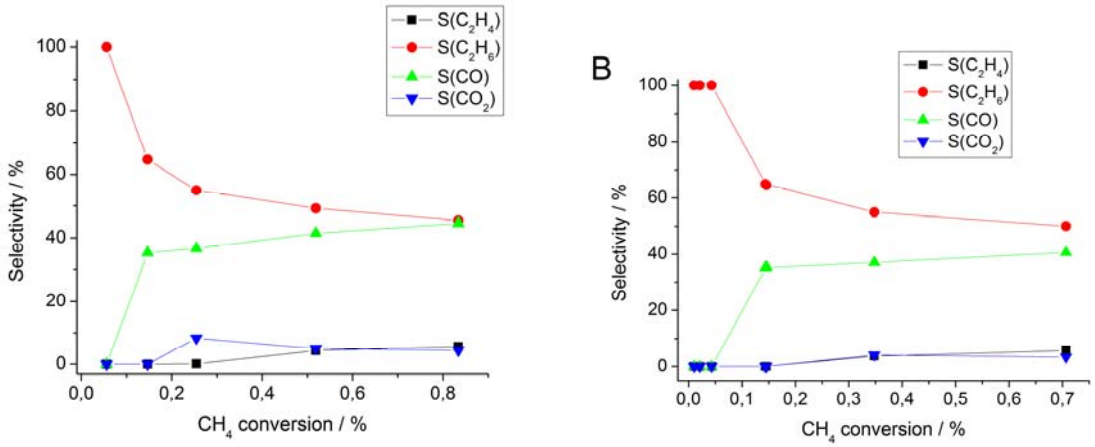

Fig. 8. Total selectivity to the coupling products ethane and ethylene over SiC as a function of methane conversion measured by variation of the contact time (A) (same condition as in Fig. 7) and by variation of the temperature (B) (same condition as in Fig. 10).

With decreasing oxygen concentration in the feed, the C_{2+} selectivity decreases for all catalysts (Fig. 9A). The reaction orders with respect to CH_4 at fixed O_2 concentration, and with respect to O_2 at fixed CH_4 concentration are summarized in Table 5. The results indicate that the overall reaction rate is almost independent from the methane partial pressure but that the oxygen partial pressure plays an important role in the OCM reaction over MgO under the explored reaction conditions. For all the catalysts an increase in the CH_4/O_2 ratio leads to a decrease in methane conversion, as well as CO_2 and C_2H_4 selectivity (results exemplarily shown for C-MgO in Fig. 9B). In contrast, the selectivity to ethane and carbon monoxide increase with decreasing oxygen partial pressure in the feed. These opposite trends for CO and CO_2 indicate that the two products are formed via different pathways (see also Fig. 6B).

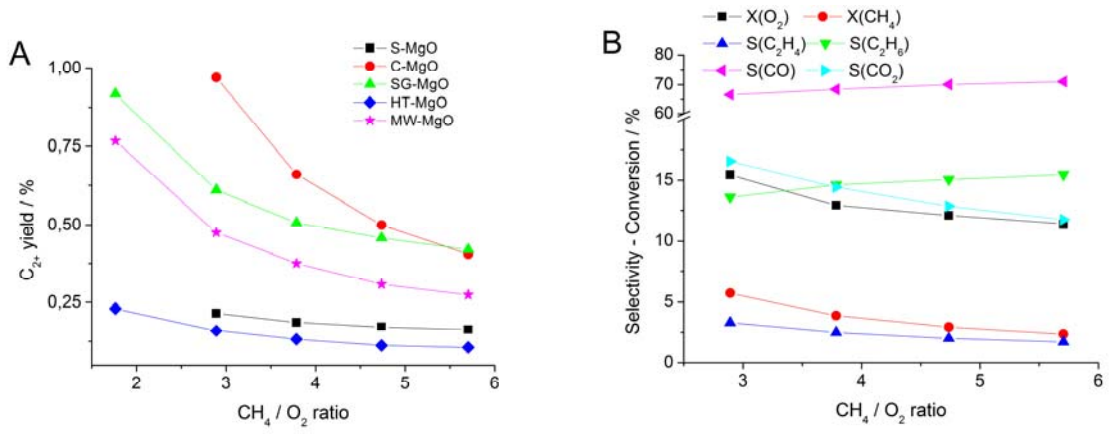

Fig. 9. Total yield of the coupling products ethane and ethylene (A), and conversion and selectivity exemplarily shown for catalyst C-MgO (B) as a function of the CH_4/O_2 ratio in the feed at T=1023 K using a catalyst mass of m_{cat}=150 mg, and a contact time of 0.15 g·s·ml^{-1}.

The temperature has a major effect on the OCM reactivity. By increasing the temperature from 873 K up to 1073 K, the yield of C_{2+} hydrocarbons increases exponentially (Fig. 10A). The apparent activation energies calculated based on the rate of methane consumption for the five catalysts are shown in Table 5. The synthesis and deactivation history of MgO have a significant impact on the apparent activation energy measured under steady-state conditions that varies between 100 kJ·mol^{-1} for C-MgO and 156 kJ·mol^{-1} for HT-MgO although all catalysts lost their high initial activity and approach similar performance in the steady-state (Table 4). Much higher activation energy is measured over SiC (297 kJ·mol^{-1}) where gas-phase reactions prevail. Here, only ethane is formed up to 998 K, at 1023 K carbon monoxide starts to occur and ethylene and carbon dioxide appear in the product mixture at temperatures higher than 1048 K. These observations are in agreement with a reaction network dominated by gas-phase reactions, in which ethylene is a consecutive product formed from ethane, CO is the major oxidation product, whereas CO_2 is formed only in small amounts.[21] Thus, MgO as a catalyst clearly lowers the energy barrier of methane activation by at least 150 kJ·mol^{-1} in comparison to the gas phase reaction. The initial rates of methane consumption increase

with decreasing apparent activation energy except for S-MgO in the order C-MgO>MW-MgO>SG-MgO>HT-MgO>S-MgO.

Table 5: Kinetic parameters measured over MgO catalysts in oxidative coupling of methane in the ***steady-state***. The apparent activation energies E_a were determined based on the methane consumption rate in the temperature range T=923-1073 K applying a contact time of 0.15 g·s·ml^{-1}, and a feed composition of $CH_4/O_2/N_2$=3/1/1. The apparent reaction orders n_{app} were determined at T= 1023 K at a contact time of 0.15 g·s·ml^{-1} and variation of the CH_4/O_2 ratio from 0.75 to 3.6 and the O_2/CH_4 ratio from 3 to 6; The initial rates of methane consumption were obtained by extrapolation to W/F=0 under steady-state conditions at 1023 K, and a CH_4/O_2 ratio of 3.

Catalyst	E_a (r_{CH4}) [kJ·mol^{-1}]	$n_{app}(CH_4)$	$n_{app}(O_2)$	Initial rate of CH_4 consumption [µmol·g_{cat}^{-1}·s^{-1}]
S-MgO	139±3	0.4	0.7	5.90
C-MgO	100±5	0.0	1.0	12.45
SG-MgO	133±2	0.3	0.8	9.56
HT-MgO	156±2	0.4	0.7	6.94
MW-MgO	119±3	0.1	0.9	10.06
SiC	297±13	n.d.	n.d.	n.d.

With increasing temperature, the selectivity towards C_{2+} hydrocarbons and CO_2 increases, which is the same trend as observed with increasing methane conversion (results exemplarily shown for C-MgO in Fig. 10B). The increase in selectivity with temperature is consistent with the thermodynamics of the selective and non-selective reaction steps in methane oxidation.[5]

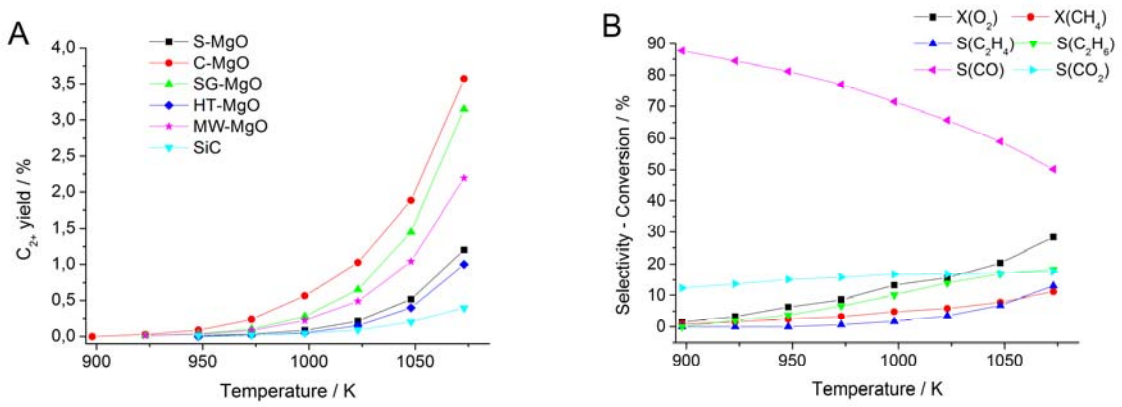

Fig. 10. Total yield of the coupling products ethane and ethylene (A), and conversion and selectivity exemplarily shown for C-MgO (B) as a function of the temperature using

a catalyst mass of m_{cat}=150 mg, a contact time of 0.15 g·s·ml^{-1} and a feed composition of $CH_4/O_2/N_2$=3/1/1.

The stability of the products ethane, ethylene, and carbon dioxide and there influence on the reaction network have been investigated by addition of 1 to 5 vol% of these gases to the feed under standard steady-state condition, *i.e.,* T=1023K, CH_4/O_2 ratio = 3, W/F=0.150 g·s·ml^{-1}, using nitrogen as balance. Since reaction products are co-fed, it is not possible to determine the selectivity. Therefore, partial pressures of the effluent gas components measured by gas chromatography are presented in Fig. 11 as a function of the concentration of ethane added to the feed. The straight black line represents the amount of ethane that should be measured at the outlet of the reactor if no added ethane would react at all. In agreement with the observations made by Roos et al. for Li/MgO catalysts [22], C_2H_6 is not stable in the OCM feed under standard condition. It should be noted that the conversion of co-fed ethane is comparable over SiC and MgO (Fig. 11). Also the product distributions are similar over MgO (Fig. 12A) and SiC (Fig. 12B). Ethane is partially oxidized to carbon monoxide and transformed into C_2H_4 to a considerable fraction. Methane conversion is only slightly affected. Hence, a competition between ethane conversion reactions and oxidative coupling of methane is not obvious. The results indicate that ethane co-added to the feed under ***steady-state*** conditions mainly reacts through gas phase chemistry.

In contrast to ethane, ethylene is more stable when added to the OCM feed. This observation is consistent with the higher dissociation energy of the C-H bond in ethylene (464.2 kJ·mol^{-1}) compared to ethane (420.5 kJ·mol^{-1}), respectively.[23] Only C-MgO and SG-MgO are able to convert slightly more ethylene than SiC (Fig. 13A). After addition of 5% ethylene over C-MgO, conversion of methane and oxygen, as well as the concentration of CO_2, C_2H_6 and CO

increase approximately by a factor of 2 (Fig. 13B). This differs from the results of Roos *et al*.,[22] who reported a decrease in methane conversion after ethylene addition. However, in the latter work the catalyst was operated under conditions of complete oxygen consumption. In this case, OCM and ethylene oxidation reactions compete for the oxygen in the feed. The present increase in methane conversion may be caused by an increase in the pool of radicals due to the reaction of added ethylene.

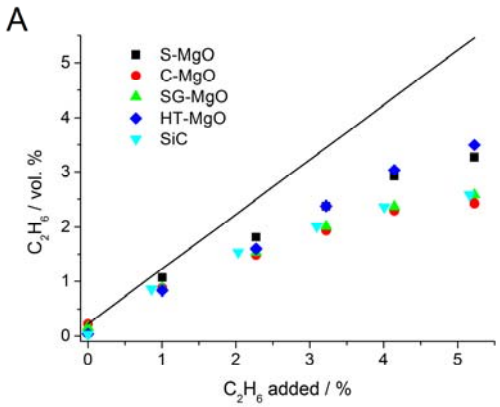

Fig. 11. Concentration of ethane measured at the outlet of the reactor for all catalysts as a function of ethane added to the feed at T=1023 K, a CH_4/O_2 ratio of 3, and a constant contact time of 0.15 g·s·ml^{-1}. The black straight line corresponds to zero conversion of the added ethane.

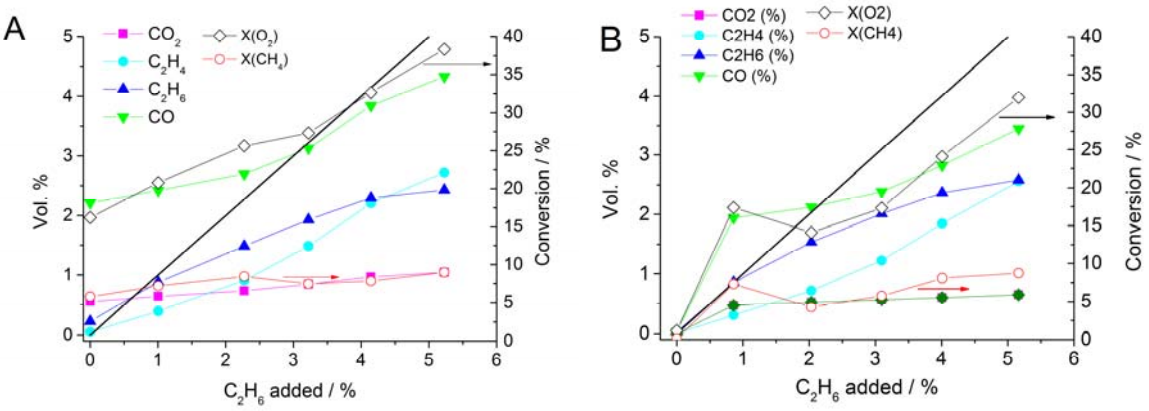

Fig. 12. concentration of all products as well as methane and oxygen conversion exemplarily shown for catalyst C-MgO (A) and SiC (B) as a function of ethane added to the feed at T=1023 K, a CH_4/O_2 ratio of 3, and a constant contact time of 0.15 g·s·ml^{-1}. The black straight line corresponds to zero conversion of the added ethane.

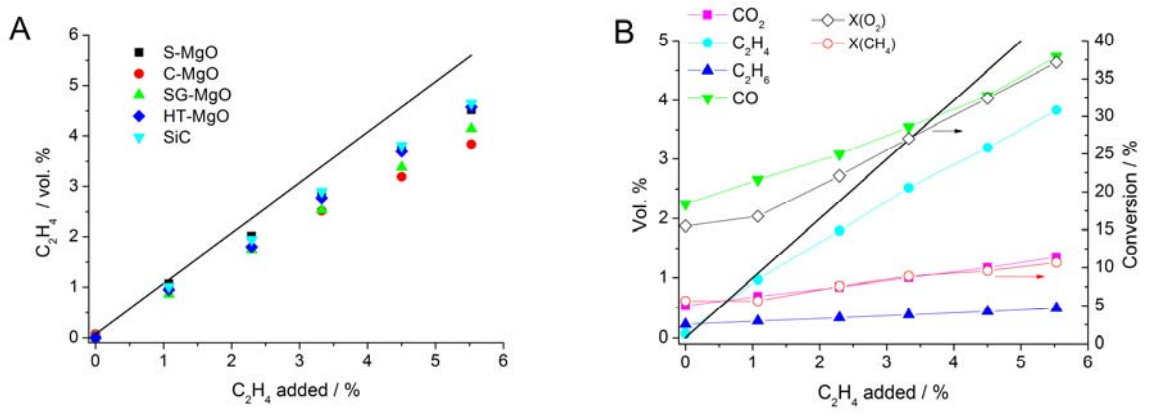

Fig. 13. Concentration of ethylene measured at the outlet of the reactor for all catalysts (A), and concentration of all products as well as methane and oxygen conversion exemplarily shown for catalyst C-MgO (B) as function of ethylene added to the gas feed at T=1023 K, a CH_4/O_2 ratio of 3, and a constant contact time of 0.15 g·s·ml^{-1}. The black straight line corresponds to zero conversion of the added ethylene.

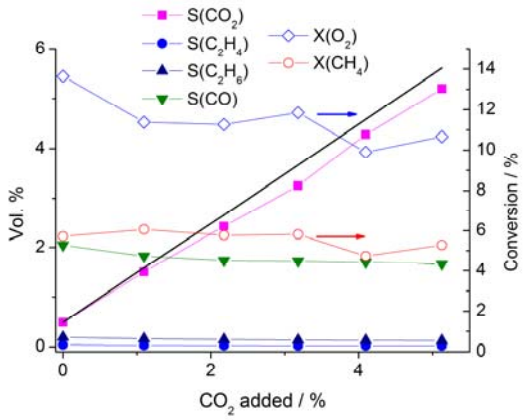

Fig. 14. Methane and oxygen conversion and concentration of products as function of CO_2 added to the feed over C-MgO at T=1023 K, a CH_4/O_2 ratio of 3, and a contact time of 0.15 g·s·ml^{-1}.

The addition of CO_2 to the feed at 1023 K is associated with only slight decrease in the oxygen conversion (Fig. 14). Methane conversion, and CO, CO_2, C_2H_4 and C_2H_6 concentration stay stable upon addition of 5 vol.% CO_2. These results indicate that neither dry reforming of methane occurs over MgO under these experimental conditions nor that CO_2 is a poison for the active sites responsible for methane activation.[5] Moreover, no indication was

found that the selectivity of C_2 products is favored by the presence of CO_2 in the feed as suggested in case of Li/MgO catalysts. [24] [22]

4. Discussion

MgO catalysts exhibiting different materials properties, like mean crystallite size, particle size, surface area, and concentration of surface defects were compared in view of their reactivity in the oxidative coupling of methane. The importance of structural aspects in the oxidative coupling of methane over magnesium oxide has been reported previously.[8] Hargreaves *et al.* studied the morphology of three differently prepared MgO catalysts by transmission electron microscopy and the results were correlated with steady-state catalyst performance in the oxidative coupling of methane, resulting in the conclusion that the active sites are mainly located on the planar {100} surfaces and not on steps or corners. Magnesium oxide, which exposed a greater fraction of higher index planes, like {111}, was particularly selective, indicating that a number of different active centers contribute to the catalytic performance on nanostructured MgO.

In the present work, variability in particle morphology and nano-structure of the MgO surface was achieved by applying different synthesis methods and post-treatment procedures of commercially available MgO, respectively. Although all investigated catalysts are chemically composed of the same binary compound (Table 1), the materials exhibit interesting differences in their reactivity in oxidative coupling of methane in particular in a very active state after short time on stream. An impact of the transition metal impurities (Table 2) on the catalytic properties can be excluded. This becomes in particular obvious from comparison of the catalysts C-MgO, HT-MgO, and MW-MgO, which are derived from the same mother MgO, having, therefore, very similar concentration of metal impurities, but show substantial differences in their catalytic

behavior. Accordingly, these differences are probably associated with different surface termination or defect concentration of the magnesium oxides, but not with the impurities.

Magnesium oxide is not stable in OCM with time on stream. The deactivation rate varies for the different MgO catalysts (Figs. 2-4) and depends apparently on the synthesis method, and, therefore, on the initial nanostructure. Along with the decrease in methane and oxygen conversion, the selectivity towards coupling products changes in favor of ethane (Fig. 3A and 4). At the same time, the total oxidation to CO_2 is inhibited resulting in an increased amount of CO in the product mixture. CO is a typical gas-phase reaction product.[21] Therefore, this observation might indicate a change in the reaction mechanism from a surface or surface-mediated reaction to a predominantly gas-phase controlled reaction. In parallel with deactivation, drastic changes in catalyst morphology are observed. Sintering is detected by XRD (Table 1) and electron microscopy (Figs. 1, 5 and S1). The surface termination becomes more regular, which is expressed in the disappearance of the mono-atomic steps, which are quite abundant in the fresh catalysts (Fig. 1).[1]

Still, some differences are retained in the steady-state reflected in different rates of methane consumption and product formation (Table 4), as well as apparent activation energies that vary from about 100 to 150 $kJ \cdot mol^{-1}$ (Table 5) depending on the catalyst preparation. Since all five catalysts are composed of magnesium oxide only, such differences in the apparent activation energy are indeed surprising. The kinetic investigation under steady state conditions described in Section 3.2.3 indicates that CO_2 and CO are probably formed via parallel pathways, which may result in different apparent activation energies calculated based on the consumption rate of methane when

the concentration of the corresponding active sites involved in rate determining steps is very different on the catalyst surface under steady state conditions.[25] In addition, varying contributions to gas phase chemistry, which are reflected in an increase in the observed apparent activation energy, cannot be excluded. Comparison of Fig. 2A with Figs. 3A and B, respectively, reveals that the ethylene/ethane ratio changes in parallel to methane conversion, but the CO_2/CO ration shows a completely different behavior, which may be interpreted in terms of a change in the reaction pathway with time on stream.

The reaction kinetics of the oxidative coupling of methane over alkaline earth oxides, whether pure or doped with alkaline elements, have been studied frequently.[26-35] Generally, it is proposed that the reaction is initiated heterogeneously on the catalyst surface and continued as homogeneous reaction in the gas phase.[5] The initial step of the selective coupling of two methane molecules is assumed to be the surface-mediated hydrogen atom abstraction from CH_4 according to an Eley-Rideal-type reaction between oxygen adsorbed on the catalyst surface and methane reacting from the gas phase.[30] Surface O^- centers are supposed to be responsible for hydrogen abstraction,[4] which yields a neutral methyl radical that is released into the gas phase for further reactions. Kinetic isotope effect (KIE) studies suggested the involvement of a C-H bond scission in the rate-determining step over Li/MgO as catalyst.[36] However, it has also been observed that the KIE decreases with increasing methane to oxygen ratio, which indicates that a single rate-determining step does not exist when oxygen is used as oxidizing agent.[37] These findings are in agreement with the varying apparent activation energy measured over the MgO catalyst series in the present work and the interpretation in terms of the parallel occurrence of independent reaction pathways that cause methane consumption. Accordingly, the apparent reaction order with respect to

methane and oxygen also differ for the different catalysts (Table 5). Furthermore, the yield of C_{2+} hydrocarbons increases with increasing methane and oxygen consumption (Fig. 7A), which would be consistent with the comparatively low sticking coefficient of methyl radicals determined on MgO that has been associated with limited consecutive surface reactions of these radicals towards undesired products of total oxidation.[31, 38] However, the contributions of homogeneous and heterogeneous reaction steps that follow the formation of the methyl radical and that determine the selectivity of the reaction are less clear.[26, 31] Analogous uncertainties exist in the literature with respect to the nature of oxygen species that are involved in the reactions. There is no doubt that oxygen is required for selective methane coupling. The oxygen partial pressure has a strong impact on the overall rate of the reaction over pure magnesium oxide as reflected in O_2 reaction orders close to one in the steady-state (Table 5). When the reaction is performed under such conditions that the oxygen consumption at *t=0* is not complete, a linear dependency of the rate of methane consumption at very short times on stream (not under steady-state conditions) on the conversion of oxygen is observed for the different catalysts (Fig. 15). This holds also for the rate of C_{2+} formation. These observations suggest that on the fresh catalyst in the initial state of the reaction the selective activation of methane towards the formation of C_{2+} hydrocarbons is directly linked with the consumption of oxygen.

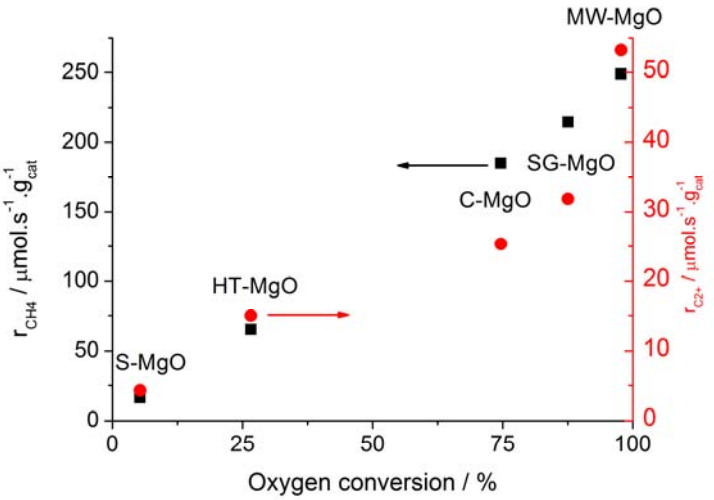

Fig. 15. Effect of oxygen conversion on the rate of methane conversion and C_{2+} formation at time *t=0* h. For reaction conditions, see Table 3.

The experimentally observed fact that the oxygen partial pressure has a significant influence on the reaction rate indicates that methane and oxygen activation are strongly correlated. Therefore, we postulate a model for C_{2+} formation on the surface of pure, nano-structured and dehydroxylated MgO that differs from the general picture of an Eley-Rideal mechanism, which involves activated O^- species adsorbed on the surface (which have so far not been verified experimentally under reaction conditions) and methane reacting from the gas phase. We assume that methane molecules are polarized by adsorption on MgO. These weakly adsorbed CH_4 molecules undergo a concerted reaction with weakly coadsorbed oxygen as illustrated in Scheme 1. On the surface of the fresh, dehydroxylated catalyst, many steps occur (1). Two methane molecules adsorb simultaneously at such a step (2). At the same time, an oxygen molecule approaches the surface close to the adsorbed methane molecules and is polarized as well (3). Next, in a concerted process, one hydrogen atom is abstracted from each of the methane molecules by oxygen forming at the same time hydrogen peroxide and ethane adsorbed at the MgO surface by creating two O-H and one C-C bond (4). Hydrogen peroxide is able to oxidize

directly the formed ethane resulting in ethylene and water (5). Finally ethylene and water desorb leaving a clean MgO surface (1). Alternatively, a methyl radical can be formed in step (3) by interaction of an adsorbed oxygen molecule with only one methane molecule, resulting in the formation of an O_2^- radical and a proton, which can combine to perhydroxyl radicals HO_2^- that may contribute together with the methyl radical to the gas phase chemistry.

The mechanistic concept proposed in Scheme 1 provides an explanation for the high reaction temperatures that are required, which is, apparently, in conflict with the observation that methane can be activated already at room temperature on the surface of MgO.[9] Perhydroxyl radicals are precursors for the formation of hydroxy groups and water, and water itself may hydroxylate MgO, which may lead to deactivation of the MgO catalysts by sintering. Once the surface is covered with adsorbed hydroxy groups, methane cannot adsorb anymore, unless high reaction temperatures are applied to assure a partially dehydroxylated surface under reaction conditions. In addition, Ito *et al.* reported that methyl radicals from the gas phase could react with surface oxygen under formation of strongly bonded methoxide species. Lunsford *et al.* confirmed that the sticking coefficient of methyl radicals on metal oxide surfaces drastically increase in the presence of oxygen in the gas phase due to the formation of methoxide ions.[39] Methoxide species can be transformed into carbonates at room temperature and decompose only at high temperature (T > 700 K) to produce either syngas or carbon dioxide and water.

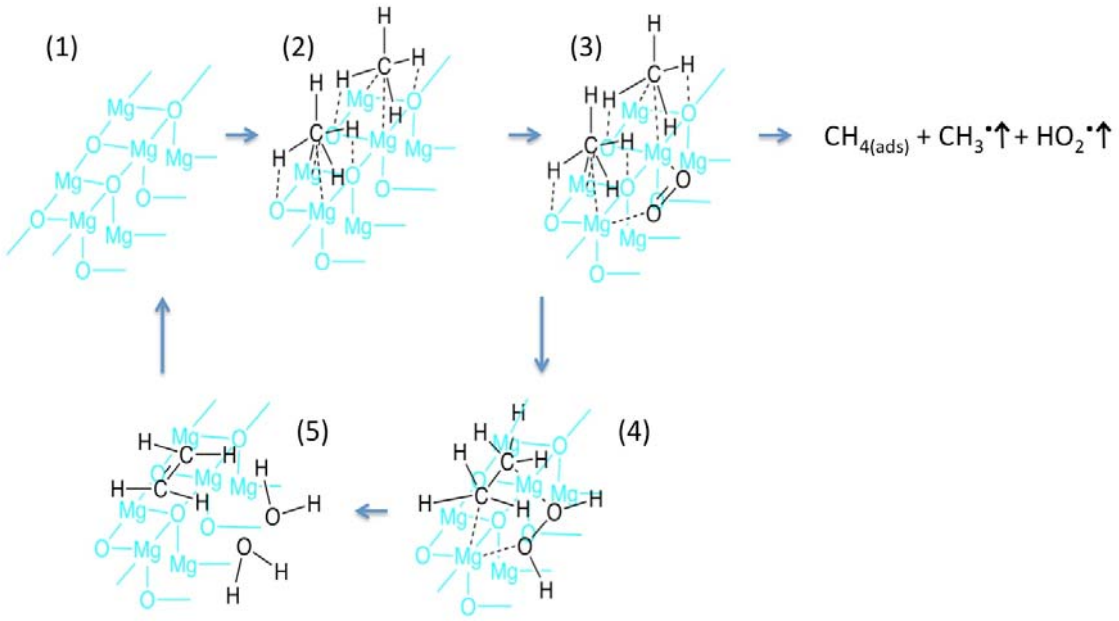

Scheme 1. Hypothetical reaction mechanism of the formation of C_2 products in the oxidative coupling of methane over freshly activated MgO catalysts after short times on stream.

There are several common characteristics between the reactivity in the OCM reaction on the fresh catalyst at time *t=0* and the kinetics at steady state. The most important similarity is the strong correlation between methane consumption and oxygen conversion (Fig. 15, Table 3). High methane conversion is accompanied by high oxygen consumption and, consequently, high C_{2+} selectivity. The same correlation is observed between the C_2H_4 / C_2H_6 and CO_2 / CO ratios and the activity (Fig. 3).

Several arguments support the surface mediated ethylene formation mechanism as proposed in Scheme 1. These experimental observations are the following:

- The observation that ethane formation is rather independent of the contact time, but ethylene selectivity increases with increasing contact time (Fig. 6B, Figs. S2-S5) excludes that a consecutive mechanism dominates (formation of ethylene by oxidative dehydrogenation of desorbed and re-adsorbed ethane), and implies that two different mechanisms occur in parallel: (i) methane reacts according to Scheme 1 preferentially to ethylene; (ii) In step 3, a methyl radical can be formed by intermolecular charge transfer between an adsorbed, polarized methane molecule and only one oxygen molecule forming a methyl radical, a superoxide species, and a proton. The methyl radical desorbs than to the gas phase. In this case, ethane is formed through gas phase coupling of two methyl radicals in agreement with the established mechanistic view. The latter process does not depend on the contact time or only in a limited manner.

- The surface mediated coupling mechanism proposed in Scheme 1 explains also the formation of propene and propane. At longer contact times (higher conversions), a third methane molecule has time to adsorb near the ethylene (or ethane, resp.) in *statu nascendi* and form a C-C bond with the C_2 intermediate through further oxidation by reaction of another oxygen molecule with this intermediate. (Fig. 7B)

- A concerted formation of C_{2+} hydrocarbons is further supported by the comparison between the OCM reactivity over MgO and SiC. Over SiC at very low conversions, C_2H_6 is formed selectively and further oxidation is prevented, since oxygen activation is difficult or impossible on SiC. At higher conversion, mainly partial oxidation of C_2H_6 occurs. In contrast, over MgO, the catalytic surface facilitates oxygen activation. At low conversion, partial oxidation of the desorbed

reaction product C_2H_6 in the gas phase predominates (mainly CO as product), while at higher conversion, the surface mediated reaction prevails (more C_2H_4 and CO_2 as products) and the contribution of C_2H_6 partial oxidation decreases.

- The oxidative dehydrogenation of auxiliary ethane added to the OCM feed does not follow the reactivity patterns of OCM indicating that ethylene is not a consecutive product of desorbed and re-adsorbed ethane. (Figs. 7B and 12B).
- In Contrast to Li-MgO, addition of CO_2 has no poisoning effect over MgO. This suggests that point defects might not be responsible for methane activation over pure MgO since CO_2 forms rapidly CO_2^- or CO_3^- in contact with V or F centers and would compete with oxygen for adsorption sites.
- The low or zero apparent reaction order with respect to methane is not in agreement with the abstraction of a hydrogen atom by an O^- center and an Eley-Rideal-type mechanism. In the case of pure MgO catalysts the limiting steps appears to be the activation of oxygen, *i.e.,* the formation of perhydroxyl radicals.

With the reaction mechanism presented in Scheme 1 we introduce a hypothesis that is based on the analysis of the kinetic data, and electron microscopy, which shows that the most reactive catalysts exhibit small cubic primary particles terminated by {100} planes with steps on their surfaces. Since it is energetically not probable that methane adsorbs on {100} terrace sites and since we ruled out point defects as active centers, the OCM reaction probably takes place on steps present on freshly activated, dehydroxylated MgO {100} surfaces. The nature of these catalytically active sites will be analyzed by spectroscopic techniques and described in detail in Part II of this work.[1]

5. Conclusions

At this point, we postulate that two different mechanisms occur in the oxidative coupling of methane over MgO catalysts: (i) “Surface-mediated coupling” characterized by high methane conversion and high C_2H_4 selectivity; and (ii) “Gas-phase coupling” involving gas phase combination of methyl radicals to C_2H_6 and C_2H_6 partial oxidation. Over fresh MgO catalysts, the surface mediated coupling mechanism is predominant. During the reaction, the primary catalyst particles sinter and the amount of active site decreases drastically, which is reflected in catalyst deactivation. While the number of active sites decreases, the contribution of gas phase chemistry increases leading to decreasing selectivity and lower activity. However the surface mediated coupling can still be observed in the deactivated steady-state, especially at long contact time (high conversion).

Acknowledgements

The authors thank Gisela Lorenz and Pia Kjaer Nielsen for their help with the surface area measurements, Dr. Frank Girgsdies and Edith Kitzelmann for performing the XRD analysis, and Iris Pieper at the Technical University Berlin for chemical analysis. This work was conducted in the framework of the COE “UniCat” (www. unicat.tu-berlin.de) of the German Science Foundation.

References

[1] P. Schwach, N. Hamilton, M. Eichelbaum, L. Thum, T. Lunkenbein, R. Schlögl, A. Trunschke, Journal of Catalysis, submitted (2015).
[2] U. Zavyalova, M. Holena, R. Schlögl, M. Baerns, ChemCatChem, 3 (2011) 1935-1947.
[3] T. Ito, J.H. Lunsford, Nature, 314 (1985) 721-722.
[4] D.J. Driscoll, W. Martir, J.X. Wang, J.H. Lunsford, Journal of the American Chemical Society, 107 (1985) 58-63.
[5] Kondratenko E. V., B. M., Handbook of Heterogeneous Catalysis in: K.H. Ertl G., Schüth F., Weitkamp J. (Ed.) Oxidative Coupling of Methan, Wiley-VCH, 2008, pp. 3010-3023.
[6] J.H. Lunsford, M.D. Cisneros, P.G. Hinson, Y. Tong, H. Zhang, Faraday Discussions of the Chemical Society, 87 (1989) 13-21.
[7] U. Zavyalova, M. Geske, R. Horn, G. Weinberg, W. Frandsen, M. Schuster, R. Schlögl, ChemCatChem, 3 (2011) 949-959.
[8] J.S.J. Hargreaves, G.J. Hutchings, R.W. Joyner, C.J. Kiely, Journal of Catalysis, 135 (1992) 576-595.

[9] T. Ito, T. Watanabe, T. Tashiro, K. Toi, Journal of the Chemical Society-Faraday Transactions I, 85 (1989) 2381-2395.
[10] M. Sterrer, M. Heyde, M. Novicki, N. Nilius, T. Risse, H.-P. Rust, G. Pacchioni, H.-J. Freund, The Journal of Physical Chemistry B, 110 (2006) 46-49.
[11] M. Sterrer, E. Fischbach, T. Risse, H.-J. Freund, Physical Review Letters, 94 (2005) 186101.
[12] H.-M. Benia, P. Myrach, A. Gonchar, T. Risse, N. Nilius, H.-J. Freund, Physical Review B, 81 (2010) 241415.
[13] N.A. Richter, S. Sicolo, S.V. Levchenko, J. Sauer, M. Scheffler, Physical Review Letters, 111 (2013) 045502.
[14] Y. Cui, X. Shao, M. Baldofski, J. Sauer, N. Nilius, H.-J. Freund, Angewandte Chemie International Edition, 52 (2013) 11385-11387.
[15] P. Schwach, M.G. Willinger, A. Trunschke, R. Schlögl, Angewandte Chemie International Edition, 52 (2013) 11381-11384.
[16] S. Utamapanya, K.J. Klabunde, J.R. Schlup, Chemistry of Materials, 3 (1991) 175-181.
[17] F. Kapteijn, J.A. Moulijn, Laboratory Catalytic Reactors: Aspects of Catalyst Testing, in: Handbook of Heterogeneous Catalysis, Wiley-VCH Verlag GmbH & Co. KGaA, 2008.
[18] CRC Handbook of Chemistry and Physics, 77th Edition, CRC Press, 1996.
[19] S. Stankic, M. Cottura, D. Demaille, C. Noguera, J. Jupille, Journal of Crystal Growth, 329 (2011) 52-56.
[20] D. Schweer, L. Meeczko, M. Baerns, Catalysis Today, 21 (1994) 357-369.
[21] O. Korup, S. Mavlyankariev, M. Geske, C.F. Goldsmith, R. Horn, Chemical Engineering and Processing: Process Intensification, 50 (2011) 998-1009.
[22] S.J. Korf, J.A. Roos, N.A. de Bruijn, J.G. van Ommen, J.R.H. Ross, Journal of the Chemical Society, Chemical Communications, (1987) 1433-1434.
[23] K. Aika, J.H. Lunsford, The Journal of Physical Chemistry, 81 (1977) 1393-1398.
[24] J.H. Lunsford, Angewandte Chemie International Edition in English, 34 (1995) 970-980.
[25] K.P. Peil, J.G. Goodwin Jr, G. Marcelin, Journal of Catalysis, 131 (1991) 143-155.
[26] P.M. Couwenberg, Q. Chen, G.B. Marin, Industrial & Engineering Chemistry Research, 35 (1996) 3999-4011.
[27] E. Iwamatsu, K.-I. Aika, Journal of Catalysis, 117 (1989) 416-431.
[28] Y.K. Kao, L. Lei, Y.S. Lin, Industrial & Engineering Chemistry Research, 36 (1997) 3583-3593.
[29] L. Mleczko, M. Baerns, Fuel Processing Technology, 42 (1995) 217-248.
[30] R.H. Nibbelke, J. Scheerova, M.H.J.M. Decroon, G.B. Marin, Journal of Catalysis, 156 (1995) 106-119.
[31] C. Shi, M. Hatano, J.H. Lunsford, Catalysis Today, 13 (1992) 191-199.
[32] J. Sun, J.W. Thybaut, G.B. Marin, Catalysis Today, 137 (2008) 90-102.
[33] J.W. Thybaut, J. Sun, L. Olivier, A.C. Van Veen, C. Mirodatos, G.B. Marin, Catalysis Today, 159 (2011) 29-36.
[34] G.J. Tjatjopoulos, I.A. Vasalos, Catalysis Today, 13 (1992) 361-370.
[35] J.M.N. van Kasteren, J.W.M.H. Geerts, K.v. der Wiele, Methane Oxidative Coupling Using Li/MgO Catalysts: The Importance of Consecutive Reactions, in: K.J.J. A. Holmen, S. Kolboe (Eds.) Studies in Surface Science and Catalysis, Elsevier, 1991, pp. 139-146.
[36] N.W. Cant, E.M. Kennedy, P.F. Nelson, The Journal of Physical Chemistry, 97 (1993) 1445-1450.
[37] C. Shi, M. Xu, M.P. Rosynek, J.H. Lunsford, The Journal of Physical Chemistry, 97 (1993) 216-222.
[38] Y. Tong, J.H. Lunsford, Journal of the American Chemical Society, 113 (1991) 4741-4746.

[39] M.T. Xu, T.H. Ballinger, J.H. Lunsford, Journal of Physical Chemistry, 99 (1995) 14494-14499.